Biomaterials 233 (2020) 119729

Contents lists available at ScienceDirect

Biomaterials

journal homepage: www.elsevier.com/locate/biomaterials

Characterization of silk-hyaluronic acid composite hydrogels towards vitreous humor substitutes

Nicole R. Raia[a], Di Jia[b], Chiara E. Ghezzi[c], Murugappan Muthukumar[b], David L. Kaplan[a,*]

[a] Department of Biomedical Engineering, Tufts University, 4 Colby St., Medford, MA, 02155, USA
[b] Department of Polymer Science and Engineering, University of Massachusetts Amherst, 120 Governors Dr., Amherst, MA, 01003, USA
[c] Department of Biomedical Engineering, University of Massachusetts Lowell, 1 University St., Lowell, MA, 01854, USA

ARTICLE INFO

Keywords:
Silk
Hyaluronic acid
Hydrogel
Vitreous humor

ABSTRACT

Multiple ophthalmic pathologies, such as retinal detachment and diabetic retinopathy, require the removal and replacement of the vitreous humor. Clinical tamponades such as silicone oil and fluorinated gases are utilized but limited due to complications and toxicity. Therefore, there is a need for biocompatible, stable, vitreous humor substitutes. In this study, enzymatically crosslinked silk-hyaluronic acid (HA) hydrogels formed using horseradish peroxidase and H_2O_2 were characterized for use as vitreous humor substitutes. The composite network structure was characterized with dynamic light scattering. In addition, the rheological, optical, and swelling properties of hydrogels with varying silk to HA ratios and crosslinking densities controlled via H_2O_2 were determined over time. Hydrogels had refractive indexes of 1.336 and were clear with 75–91% light transmission. Hydrogel shear storage modulus ranged between ~6 and 240 Pa where increased H_2O_2 increased the modulus. After 1 month of aging, there were no changes in modulus for hydrogels with lower silk ratios, while those with higher silk ratios exhibited a significant increase in modulus. Decreasing H_2O_2 concentration in the reactions led to increased hydrogel volume during swelling, with higher silk ratios returning to their original size after 15 days. Dynamic light scattering results show three diffusive modes, revealing the possible structures of the hydrogel composite and are consistent with the mechanical properties and swelling results. The normalized intraocular pressure of *ex vivo* porcine eyes after injecting hydrogels were comparable with those treated with silicone oil showing the potential clinical utility of the hydrogels as vitreous substitutes. The versatility of the silk-HA hydrogel system, the tunable swelling properties, and the stability of hydrogels with lower silk ratios show the benefit of utilizing silk-HA hydrogels as vitreous substitutes.

1. Introduction

The vitreous humor is a clear, hydrated, avascular gel consisting of randomly spaced collagen fibrils entangled within a hyaluronan bulk matrix. This network serves many functions such as maintaining ocular volume, supporting and protecting the retina, dampening mechanical inputs, and facilitating metabolite diffusion [1]. Multiple ocular diseases, such as retinal detachment and diabetic retinopathy, require the removal and replacement of the vitreous humor [2]. Clinically used tamponades, such as silicone oil and fluorinated gases, can only be utilized as short-term substitutes due to their toxicity to surrounding ocular tissues and their tendency to emulsify [3]. Therefore, there is a significant clinical need to develop improved biomaterials for substitution of the vitreous humor [3].

An ideal substitute should be able to provide a tamponade effect to facilitate retinal reattachment, provide adequate mechanics (2 Pa to > 100 Pa [4–6]), optical properties similar to native vitreous humor, biocompatibility to ocular cells and tissues, prolonged and controlled biodegradation rates (ideally > 3 months [7]), and the ability to be injected through a small gauge needle [1,3,5,8,9]. Hydrogels are attractive materials for vitreous humor substitutes due to their viscoelasticity, hydrophilicity, and potential to form *in situ*. Thus, many hydrogels have been explored as vitreous humor substitutes [3], including synthetic hydrogels such as polyvinyl alcohol (PVA) [10] and poly(1-vinyl-2-pyrrolidinone) (PVP) [11]. These polymers are advantageous for this application due to their extended retention time, rheological properties, and optical clarity, but can also be toxic to ocular tissues, non-injectable, or exhibit vitreous opacification [3,12]. Natural materials, such as hyaluronic acid (HA) and collagen, are biologically similar to native vitreous humor (which consists of up to 400 μg/cm^3 of HA and

* Corresponding author.
E-mail address: david.kaplan@tufts.edu (D.L. Kaplan).

https://doi.org/10.1016/j.biomaterials.2019.119729
Received 4 July 2019; Received in revised form 7 December 2019; Accepted 22 December 2019
Available online 27 December 2019
0142-9612/

532 μg/cm^3 of collagen [1]), but have limited retention times *in vivo* due to relatively fast degradation [3]. To increase retention time, HA has been crosslinked through UV and dihydrizide resulting in biocompatible hydrogels [13], however these materials still exhibit relatively short-term stability [3]. HA has been combined with other polymers such as gellan, a microbial anionic polysaccharide, however due to the instability of the physical crosslinks, this combination was also only for short-term use [14,15].

We have previously combined HA with silk fibroin through enzymatic crosslinking using horseradish peroxidase (HRP) and H_2O_2 [16]. Silk fibroin, a protein isolated from *Bombyx mori* cocoons, has been utilized in a variety of different hydrogel formats for different applications due to its biocompatibility, mechanical tunability, and relatively slow degradation [16–27]. Silk has shown to be biocompatible through *in vivo* studies and a suitable material for sustained ocular drug delivery [28,29]. In addition, the biocompatibility of silk particles suspended in an HA hydrogel have been explored for use in soft tissue augmentation, showing minimal signs of inflammation in a rat model [30]. Silk and HA composite hydrogels can be formed through HRP/H_2O_2, by crosslinking the tyrosine residues (~5%) native to silk fibroin and tyramine-conjugated HA. The combination of these two polymers helps to overcome limitations of the singular component hydrogels and allows for further tunability. By retaining favorable properties of each polymer, the composite silk-HA hydrogel has lead to increased stability; HA improves control of water content in the composite matrix, thus, reducing the rate of hydrogel stiffening due to crystallization of the silk via beta sheet formation, and the slow proteolytic degradation of the silk improves the durability of the composite matrix [16]. Furthermore, the HRP/H_2O_2 method facilitates tunability of both rate of gelation and the mechanical properties [22,31,32]. Therefore, in this study the objective was to explore silk-HA composite hydrogels as potential vitreous humor substitutes by elucidating the network structure through dynamic light scattering and determining the effect of polymer ratio and crosslinking conditions on mechanical, swelling, and optical properties over time.

2. Materials and methods

2.1. Hydrogel formulation

Silk fibroin was isolated from *B. mori* silkworm cocoons as previously described [33]. Cut cocoons were degummed in boiling sodium carbonate (Sigma-Aldrich, St. Louis, MO) solution for 60 min. The resulting fibers were washed in deionized (DI) water and then dissolved in 9.3 M lithium bromide (Sigma-Aldrich, St. Louis, MO) for 4 h. The resulting silk fibroin solution was dialyzed against water for 3 days to remove residual lithium bromide and diluted to 4% w/v using DI or ultrapure water. Lyophilized hyaluronic acid (HA) with a 5% tyramine substitution (Corgel® powder, MW ~0.9–1.0 MDa, Lifecore Biomedical, Chaska, MN) was dissolved in hank's balanced salt solution (HBSS; without magnesium and calcium; ThermoFisher Scientific, Waltham, MA) at a concentration of 10–11 mg/mL. Silk and HA were combined with varying silk/HA (S/H) ratios (50S/50H, 25S/75S, 10S/90H) at a total concentration of 1% w/v of polymer using HBSS as dilutant. Higher ratios of silk (above 50S/50H), were not utilized due to lack of gelation. Silk and HA were covalently crosslinked enzymatically as previously described [16]. Table 1 specifies the crosslinking conditions for each sample. HRP (Type VI, Sigma-Aldrich, St. Louis, MO) concentration was adjusted to obtain gelation times between 10 and 15 min (Supplement Table S1). Three H_2O_2 (Sigma-Aldrich, St. Louis, MO) concentrations (low, medium, and high) were independently chosen for each of the ratios to alter crosslinking density resulting in a low, medium, and high average shear storage moduli of less than 30 Pa, 30–110 Pa, and above 110 Pa, respectively. HA control hydrogels were formed using a ratio of 0S/100H with the same crosslinking conditions as the 10S/90H ratio. Solutions were either kept sterile or filter sterilized prior to gelation. Components were mixed on ice and allowed to gel for 1 h at 37 °C prior to submersion in HBSS (with magnesium and calcium) unless otherwise mentioned.

Table 1
Crosslinking conditions for samples. All hydrogels contained 1% w/v polymer in HBSS with varying silk/hyaluronic acid (S/H) ratios.

Sample		H_2O_2 (x10^{-2}% v/v)	HRP (U/mL)
50S/50H	*Low*	0.05	1
	Med	0.1	
	High	0.3	
25S/75H	*Low*	0.01	0.1
	Med	0.05	
	High	0.1	
10S/90H	*Low*	0.01	0.05
0S/100H	*Med*	0.02	
	High	0.05	

2.2. Rheological Characterization

Hydrogels were allowed to gel in 60 mm petri dishes for rheological analysis. Rheological properties were assessed on hydrogels after incubation in HBSS at 37 °C for 1 and 30 days using a TA Instruments ARES-LS2 rheometer (TA Instruments, New Castle, DE) fitted with a 50 mm stainless steel upper plate and peltier bottom plate lined with 600 grit sandpaper (47185A51, McMaster-Carr, Elmhurst, IL) to prevent slippage. A preload of 0.2 N to ensure complete contact, excess hydrogel was trimmed, and silicone oil was placed around the plate to prevent evaporation during analysis. A dynamic single point test was performed at 1 Hz with 3% applied strained followed by dynamic frequency sweeps (0.1–100 rad/s at 3% strain) and strain sweeps (0.1%–500%, at 1 Hz) to ensure linear viscoelasticity.

2.3. Optical properties

The refractive indices of the hydrogels were assessed by placing a thin layer of hydrogel precursor solution or HBSS solution control onto the plate of a DANOPLUS 3 in 1 Scale Clinical Refractometer with ATC (Kibeland, Hong Kong). After 20 min at room temperature to ensure hydrogel formation, the refractive index was measured as per manufacturer instructions. The transparency of the hydrogels was characterized similarly to previous reports [15,27]. In brief, 100 μL of hydrogel solution was allowed to gel in a clear 96-well plate and incubated in HBSS for 1 day and 30 days. The percentage of light transmitted through the hydrogel for wavelengths in the visible range (400–700 nm) was determined using a SpectraMax M2 multi-mode microplate reader (Molecular Devices, Sunnyvale, CA).

2.4. Swelling

Hydrogel cylindrical plugs were prepared by placing hydrogel solutions into 8 mm pluronic-F127 coated PDMS molds. After 1–2 h incubation at 37 °C, hydrogel plugs were removed from of the molds and incubated in HBSS at 37 °C for 1 month. Volumetric measurements were performed via calipers prior to incubation and after 1, 7, 15, and 29 days. To compare different S/H ratios at the same H_2O_2 concentrations, the volume was normalized to initial measurements.

2.5. Dynamic light scattering (DLS)

Due to the dust sensitivity of DLS measurements, DLS tubes were first washed several times with pure water and acetone separately. After drying in the oven overnight, aluminum foil was used to wrap the tubes. Tubes were then further cleansed with distilled acetone through an acetone fountain setup [34,35]. All sample solutions and hydrogel

precursor solutions (silk, HA, and HRP) were slowly filtered through 220 nm PVDF hydrophilic filters to remove contaminants. To induce gelation for hydrogel samples, H_2O_2 was filtered and added. After gelation was complete, HBSS was added to the tube in excess amount on top of the hydrogel to maintain equilibrium between the hydrogel and the solution.

DLS measurements were performed on a commercial spectrometer equipped with a multi-τ digital time correlator (ALV-5000/E) using a wavelength of 514.5 nm laser light source.

The scattered intensity was measured with a photomultiplier tube attached to an ALV goniometer arm. DLS measures the intensity – intensity time correlation function $g_2(q, t)$ by means of a multichannel digital correlator and related to the normalized electric field correlation function $g_1(q, t)$ through the Siegert relation [36]. For each sample, the intensity at scattering angles 30°, 40°, 50°, 60° and 90° was correlated, and the relaxation times averaged for three different spatial locations within the samples. CONTIN method [37] and multiple exponential fitting method [38] were used to analyze the characteristic relaxation rate Γ_i at each angle. Based on $D_i = \Gamma_i/q^2$, where scattering wave vector $q = (4\pi n/\lambda)*\sin(\theta/2)$, diffusion coefficient D can be obtained.

2.6. Ex Vivo Injections

The intraocular pressure (IOP) of fresh porcine eyes (Animal Technologies, Tyler, TX) were determined using a Icare® TONOVET Plus tonometer (Icare Finland Oy, Vantaa, Finland). Using an 18G needle inserted through the sclera, 500 μL of the vitreous was removed and replaced with 500 μL of silicone oil (1000 cst, Sigma-Aldrich, St. Louis, MO) or 25S/75H med hydrogel. For hydrogel samples, gelation was initiated 5 min prior to injection and allowed to fully gel prior to measurements. IOP was measured prior to vitreous removal, after vitreous removal, and after silicone oil or hydrogel injection. Results are reported as the average normalized IOP, where values were calculated as the differences between IOP prior to vitreous removal and after vitreous removal normalized by the differences between IOP after injection and after vitreous removal.

2.7. Statistics

Data are expressed as means ± standard deviations. To determine statistical significance ($p \leq 0.05$) for rheological ($n = 3–4$) and swelling ($n = 5$) data, two-way ANOVA (analysis of variance) with Tukey's post hoc multiple comparisons were performed using GraphPad Prism (GraphPad Software, La Jolla, CA). For optical transparency ($n = 5$), data were analyzed through two-way ANOVA with Tukey post hoc multiple comparisons and comparisons over time were determined through multiple tests with the Holm-Sidak multiple comparison method. For *ex vivo* injections ($n = 5$), data were analyzed through unpaired t-tests.

3. Results

3.1. Mechanical properties

The mechanical properties of silk-HA hydrogels at varying S/H ratios and H_2O_2 concentrations were determined initially and at 1 month of incubation in physiological conditions. Concentrations of H_2O_2 were chosen for each ratio resulting in an initial shear storage modulus below 30 Pa (low), between 30 and 110 Pa (med), and above 110 Pa (high) (Fig. 1A). H_2O_2 concentration of the control hydrogels, consisting of HA only (0S/100H) with the sample conditions as for the 10S/90H samples, did not significantly affect hydrogel modulus. After 1 month, only the 50S/50H samples for all H_2O_2 concentrations exhibited a significant increase in modulus (Fig. 1B). Specifically, there was approximately a 4×, 2×, and 1.6× increase for the low, medium, and high H_2O_2 concentrations, respectively. When comparing the different S/H ratios of the same H_2O_2 concentration (Table 1), samples containing both silk and HA exhibited higher moduli with increasing HA concentration (Fig. 1C). Hydrogels with HA only controls (0S/100H) had significantly lower modulus than 10S/90H hydrogels. After 1 month, there was a similar trend with 50S/50H and 25/75H hydrogels having lower moduli than that of the 10S/90H hydrogels. In addition, at 1 month, 50S/50H hydrogels were no longer different in shear storage modulus than that of 25S/75H hydrogels. All hydrogels had linear viscoelastic regions at 3% strain (Supplement Fig. S1) and were independent of frequency except for low H_2O_2 concentration for 25S/75H, 10S/90H, and 0S/100H, which showed a slight increase in storage modulus at higher frequencies (Fig. 2).

3.2. Optical properties

All hydrogels, regardless of S/H ratio and H_2O_2 concentration, exhibited a refractive index of 1.336 compared to HBSS that has a refractive index of 1.335. The percentage of light transmitted through the hydrogels after 1 day and 1 month in physiological conditions is shown in Fig. 3. Differences between the hydrogels and the HBSS control at 500 nm are shown on the graphs. Initially the percentage of light transmittance was between 76 and 91% depending on wavelength (Fig. 3A–D). The 25S/75H low hydrogels exhibited significant differences compared to the HBSS control for all wavelengths in the visible spectra (400–700 nm) (Fig. 3B). At 1 month, the optical transparency ranged between 75 and 91% (Fig. 3E–H) with only the 50S/50H low samples differing in transparency between day 1 and 1 month between 400 and 440 nm (Fig. 3A and E). All hydrogels had some differences from the HBSS blank at 1 month, depending on wavelength. Samples that showed differences from the control for all wavelengths within the visible spectra (400–700 nm) at 1 month include 50S/50H low, 25S/75H low, and all of the 10S/90H H_2O_2 concentrations.

3.3. Swelling

Hydrogel swelling was calculated via volumetric changes initially and up to 1 month after incubating in HBSS at 37 °C (Fig. 4). For 50S/50H ratio hydrogels, low and medium H_2O_2 concentrations resulted in increased volume after 1 day, with the volume returning to the initial values after 15 and 7 days, respectively. For the 50S/50H high H_2O_2 concentration, the hydrogel volume did not change over 1 month. Similarly, 25S/75H ratio hydrogel with high H_2O_2 concentration did not exhibit volumetric changes, whereas low and medium concentrations had sustained volumetric increase throughout 1 month with volumes equilibrating at days 1 and 7 at approximately 3.6× and 1.5× the initial volume, respectively. For both 10S/90H and 0S/100H at all H_2O_2 concentrations, the volume increased and equilibrated at day 1. For 10S/90H samples at day 1, the samples were ~2.5×, 1.6×, and 1.6× their initial volume for low, medium, and high H_2O_2 concentrations, respectively. For the 0S/100H samples, the volumes were 2.1×, 1.8×, and 1.6× their initial volume for low, medium, and high H_2O_2, respectively. Comparing between ratios for the same H_2O_2 concentrations, at days 15 and 29, the 50S/50H hydrogels had a significantly lower normalized volume to all other samples.

3.4. Dynamic light scattering (DLS)

Due to the unique behavior of the 50S/50H hydrogels, we explored the internal structures of this sample as a function of time through dynamic light scattering (DLS) technique. Fig. 5 shows the intensity-intensity correlation function and its corresponding fitting results for 50S/50H hydrogel in day 1. The fitting results (Fig. 5B) shows that there are three diffusive modes with diffusion coefficients $D_1 = 4.06 \times 10^{-7}$ cm^2/s, $D_2 = 3.65 \times 10^{-8}$ cm^2/s, $D_3 = 1.31 \times 10^{-10}$ cm^2/s. Dynamic light scattering measurements

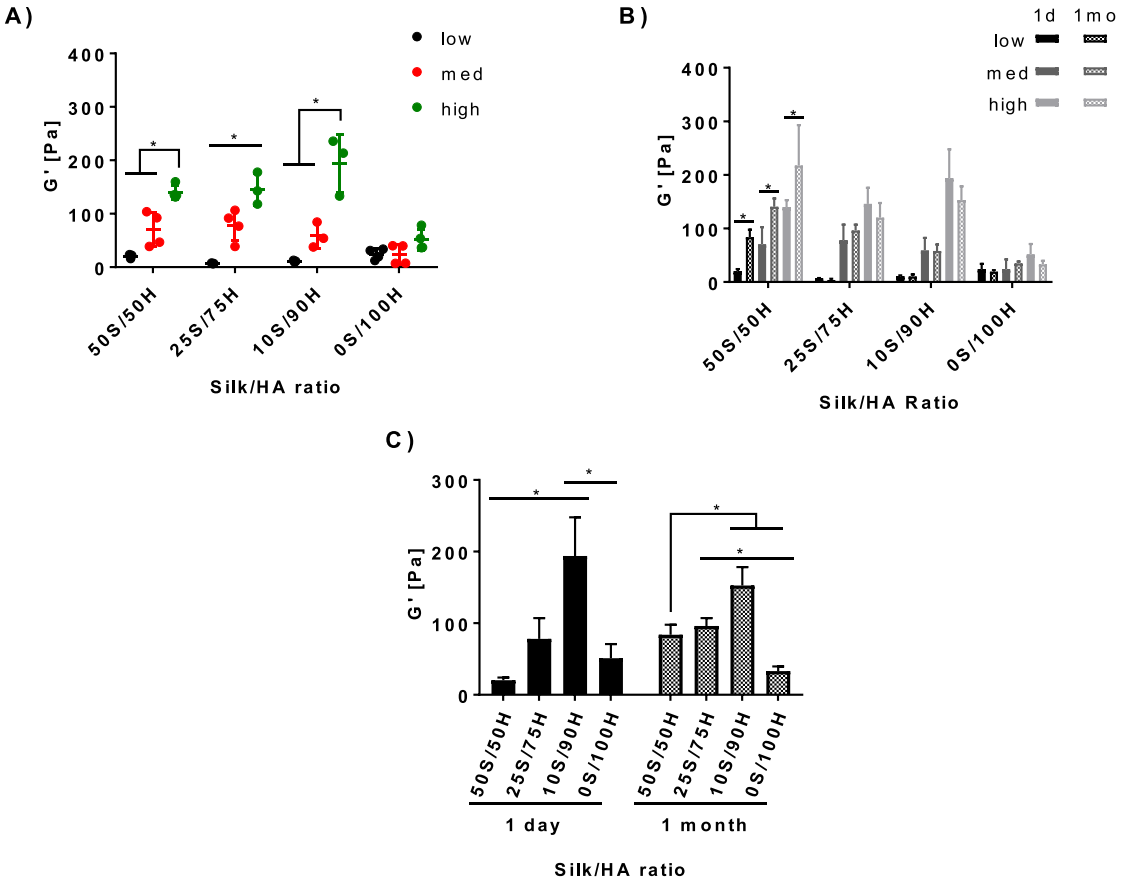

Fig. 1. Rheological Characterization: Shear Modulus. The shear storage modulus is reported for hydrogels with varying S/H ratios and H_2O_2 concentrations. The day 1 storage modulus (A) for each ratio was within a low (below 30 Pa), medium (30–110 Pa), and high (above 110 Pa) range depending on H_2O_2 concentration. Storage modulus between 1 day (solid bars) and 1 month (patterned bars) is shown for each sample (B) with 50S/50H ratios at 1 month having an 4×, 2×, and 1.6× increase in modulus for low, med, and high H_2O_2 concentrations, respectively. Comparing between ratios of similar H_2O_2 concentrations, the storage modulus at 1 day and 1 month shows a direct relationship between storage modulus and HA ratios (C). (*$p \leq 0.05$, n = 3–4).

were also conducted for the same sample after 7 days and 15 days of aging (The fitting results are in Supplement Fig. S2). The summary of the dynamic light scattering results is listed in Table 2, which shows that D_1 and D_2 increase slightly with time, while D_3 decreases with time. Finally, all the diffusion coefficients barely change by Day 15, indicating that the composite hydrogel structures have reached equilibrium.

In order to understand the three modes in the 50S/50H hydrogel composites, HA hydrogel alone and silk hydrogel alone were studied separately and compared with the results of hydrogel composite. For the HA hydrogel alone, the elastic diffusion coefficient is 3.7×10^{-7} cm^2/s (Fig. 6B), which is similar to D_1 in the 50S/50H hydrogel composite. Here the elastic diffusion coefficient of the hydrogel D = M/f (where M is the longitudinal modulus of the hydrogel, f is the friction coefficient of the hydrogel) indicates the modulus of the hydrogel [35,39]. While the elastic diffusion coefficient of the silk hydrogel alone is 4.4×10^{-8} cm^2/s, which is similar to D_2 in the 50S/50H hydrogel composite. Therefore, in the 50S/50H hydrogel composite, D_1 arises from the hydrogel elasticity of HA component and D_2 is due to hydrogel elasticity of the silk component.

Silk solution at 5 g/L was also studied. As shown in Fig. 7, there is only one mode with $D = 1.57 \times 10^{-7}$ cm^2/s. Based on Stokes-Einstein equation, we get the hydrodynamic radius R_h = 14 nm (peak position), with a broad distribution (Fig. 7B). Please note that the overlap concentration of the silk solution C* is 24.6 g/L. Therefore, for 40 g/L silk solution (C > C*), silk chains are able to contact with each other, so that once gelation occurs they can crosslink with each other to form a gel network. However, for 5 g/L silk dilute solutions (C < C*), chains are not able to contact with each other, however there is still a low chance for contact, so once they are crosslinked, silk chains will self-crosslink to form microgels. For the microgel solutions, $D = 7.58 \times 10^{-8}$ cm^2/s, R_h = 29 nm (Fig. 7D), which is double the size of silk solutions without being crosslinked.

In the 50S/50H hydrogel composite, which has the highest silk content, D_3 arises from the self-crosslinked silk microgels. Since the molecular weight of the silk is around 170 KDa [29,40], which is much smaller than that of the HA chains (Mw = 900–1000 KDa), during the gelation of the composite hydrogel, silk chains have higher mobility therefore can bond to both HA chains and bonded with other silk chains forming self-crosslinked silk microgels. Once gelation is complete, the silk-HA hydrogel matrix is formed with self-crosslinked silk microgels diffusing within the hydrogel matrix, as illustrated in the schematic of Fig. 8.

The diffusion coefficient of the silk microgels inside the 50S/50H hydrogel composite (D_3 in Table 2) is expected to be much smaller than $D = 7.58 \times 10^{-8}$ cm^2/s in the 5 g/L silk microgel solutions, because the particle is subjected to substantial friction from the background composite gel network. In fact, the diffusion coefficient for this relaxation mode becomes even smaller as the gel network gets tighter due to aging (stronger confinement). As shown in Table 2, the diffusion coefficient D_3 decreases from 1.3×10^{-10} cm^2/s (for day 1) to 2.62×10^{-11} cm^2/s (day 7) and then to 2.66×10^{-11} cm^2/s (day 15).

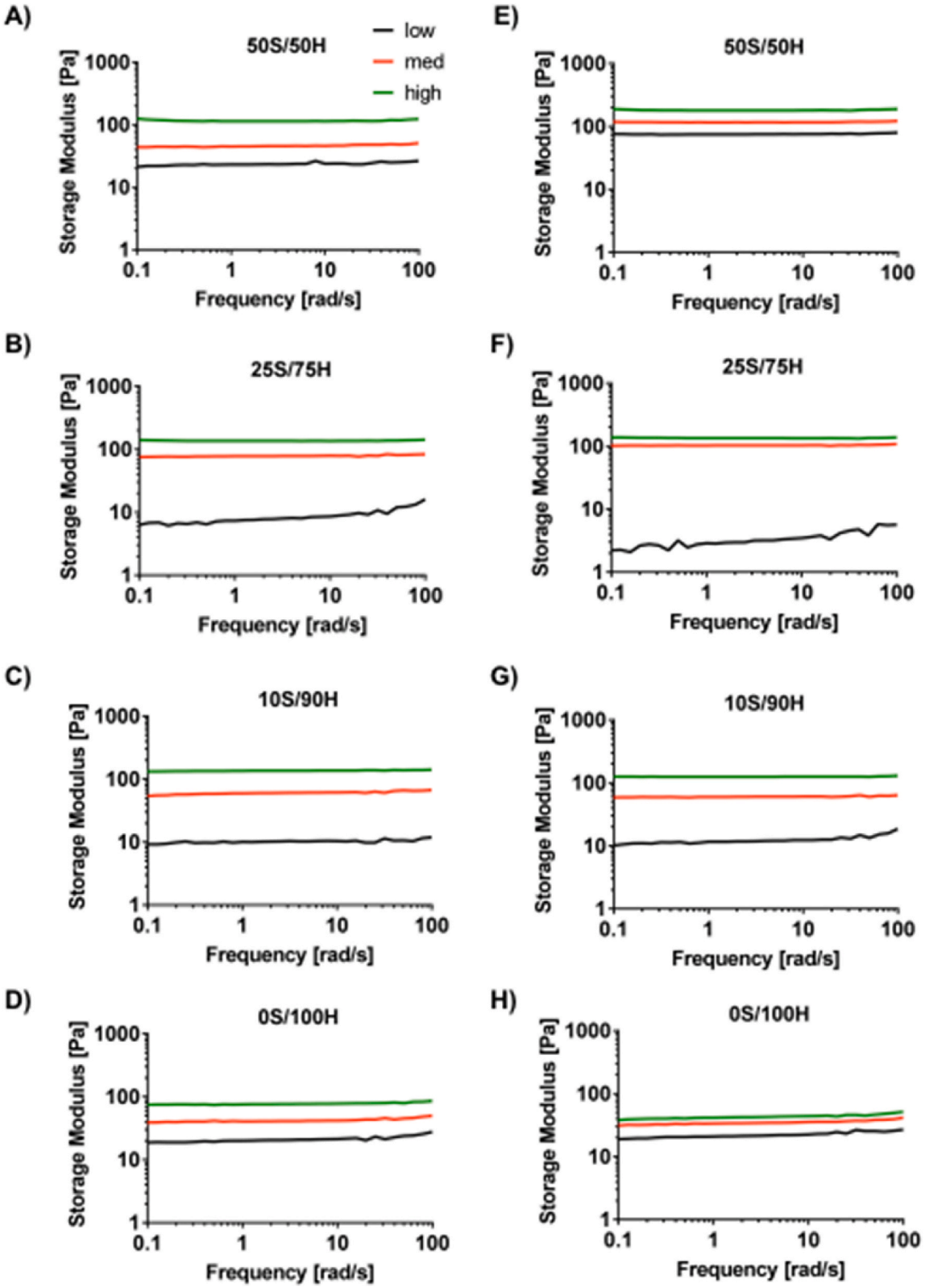

Fig. 2. Rheological Characterization: Frequency Dependency. Representative data for frequency sweeps at 3% strain of hydrogels with different S/H ratios and H_2O_2 concentrations are shown for 1 day (A–D) and 1 month (E–H). All hydrogels were frequency independent except for low H_2O_2 concentrations for 25S/75H, 10S/90H, and 0S/100H which showed a slight increase in shear storage modulus at higher frequencies.

Thus, the gel has reached its final aging state within 15 days. The dynamic light scattering results are consistent with the increase in G′ with time (G'~D_1, D_2) and the decrease in normalized volume with time for 50S/50H hydrogel composite.

3.5. Ex Vivo Injections

To determine the clinical utility of the composite hydrogels as vitreous substitutes, hydrogels (25S/75H med) were injected into *ex*

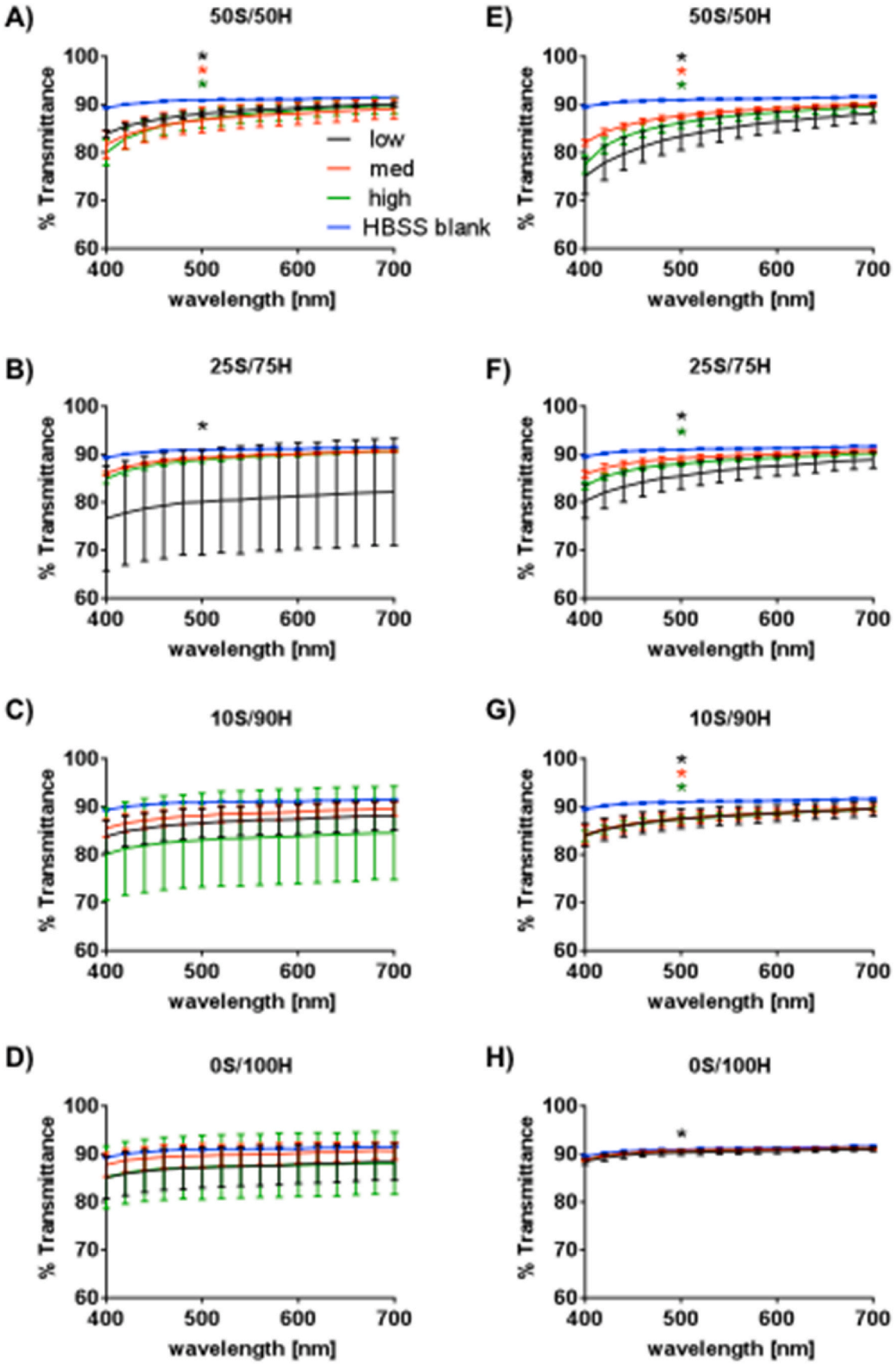

Fig. 3. Light Transmittance. Optical transparency is reported as percentage of light transmitted at day 1 (A–D) and 1 month (E–H) for each of the polymeric ratios. Statistical differences from the HBSS control at 500 nm are shown (*low (black), *med (red), *high (green), $p \leq 0.05$, $n = 5$). (For interpretation of the references to color in this figure legend, the reader is referred to the Web version of this article.)

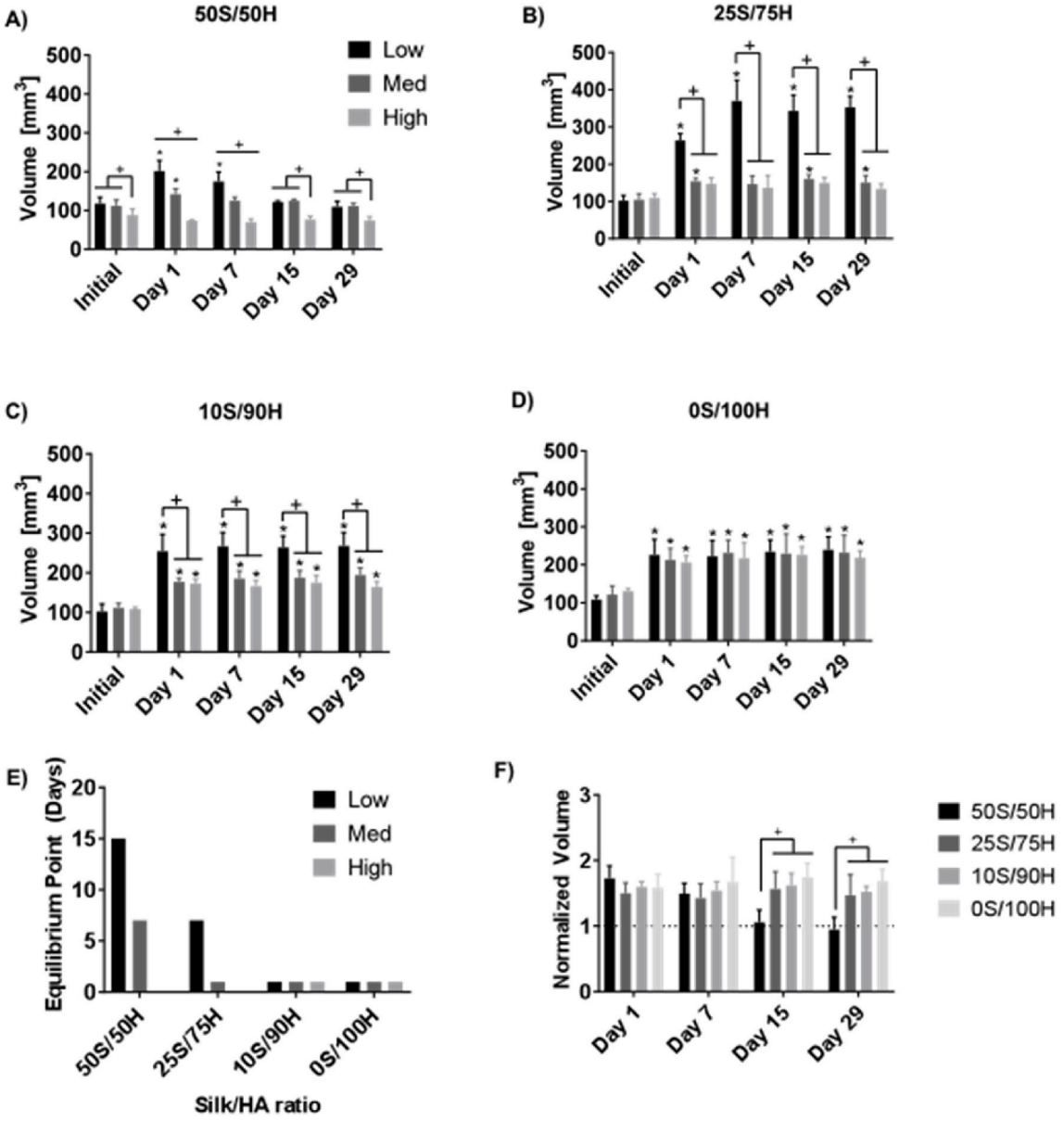

Fig. 4. Swelling. Volumes are reported for hydrogels over a 1-month period (A–D). The time at which the volume no longer changes is shown in (E) where hydrogels with increased HA concentration and higher H_2O_2 concentration equilibrated faster. When comparing between ratios of the same H_2O_2 concentration (F), the 50S/50H hydrogels had a lower normalized volume than all other ratios ($+p \leq 0.05$, $*p \leq 0.05$ compared to initial volume, $n = 5$).

vivo porcine eyes after removal of the vitreous and compared to a clinical control, silicone oil [41]. Upon gross observation, both the silicone oil and hydrogel restored initial ocular shape after the removal of the vitreous (Fig. 9A). There were no statistical differences ($p > 0.05$) between the normalized IOP of the silicone and hydrogel injected eyes (Fig. 9B).

4. Discussion

Enzymatically crosslinked silk-HA hydrogels were characterized in the context of vitreous humor substitutes. The studies focused on how altering S/H ratios and H_2O_2 concentration effected mechanical, swelling, and optical properties over time. In situ gelation is an important parameter for polymeric vitreous substitutes as it prevents fragmentation and preserves elasticity and mechanical properties [42]. Therefore, enzyme concentrations for each polymer ratio were chosen to allow gelation to occur within 10–15 min, providing adequate time for proper mixing *ex vivo*, and rapid gelation *in vivo*, to prevent migration from the delivery site. According to previous reports, altering the enzyme concentration should independently control gelation rate without affecting crosslinking density [31,32]. Using the HRP/H_2O_2 reaction, crosslinking density of phenol-conjugated polymers is independently tuned via altering H_2O_2 concentrations [31,32].

As previously discussed, ideal vitreous substitutes need to be biocompatible and also mimic native vitreous optical properties and have adequate mechanics and tunable swelling to provide an effective tamponade, restoring ocular volume and preventing retinal detachment. There has been extensive research on the mechanics of both native vitreous humor and substitute biomaterials. The mechanics of vitreous humor substitutes varies in the literature with many reports suggesting a range of native vitreous shear storage modulus (5–15 Pa) [4]. However, these values may not accurately represent the vitreous *in vivo* as the properties of the vitreous body changes upon removal [6] and the modulus of the vitreous with an intact membrane is much higher than the vitreous humor alone [43]. A polymer with higher mechanical integrity will better absorb shock, provide an effective tamponade, and

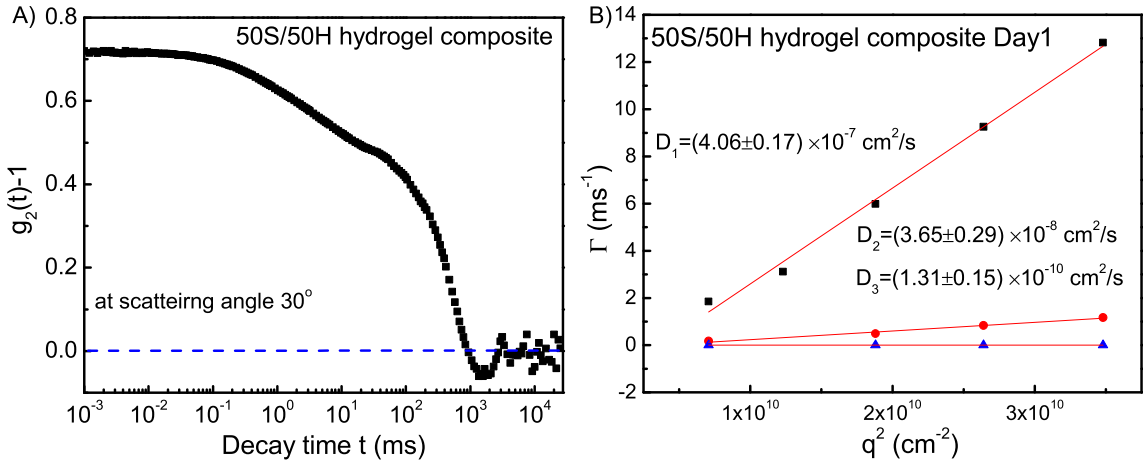

Fig. 5. (A) Intensity-intensity correlation function for 50S/50H hydrogel at scattering angle 30°. (B) q^2 dependence of the relaxation rate Γ of all the three modes for the 50S/50H hydrogel in Day 1. From the slope of Γ_i/q^2, diffusion coefficient D_i for each mode can be obtained.

Table 2
Dynamics light scattering results as a function of time for 50S/50H hydrogel. D is the diffusion coefficient.

Time	D_1 (cm^2/s)	D_2 (cm^2/s)	D_3 (cm^2/s)
Day 1	4.06E-7	3.65E-8	1.31E-10
Day 7	4.35E-7	5.68E-8	2.62E-11
Day 15	4.41E-7	5.43E-8	2.66E-11

have increased stability and retention time [6,44]. For these reasons, ideal vitreous substitutes should have shear storage moduli above 100 Pa [6]. Therefore, in this study, we characterized a range of mechanical properties to provide a versatile biomaterial for vitreous humor substitutes. For each S/H ratio tested, we chose $3H_2O_2$ concentrations (low, medium, and high), which directly relate to cross-linking density, allowing the biomaterial to exhibit shear storage moduli in three ranges; below 30 Pa, between 30 and 110 Pa, and above

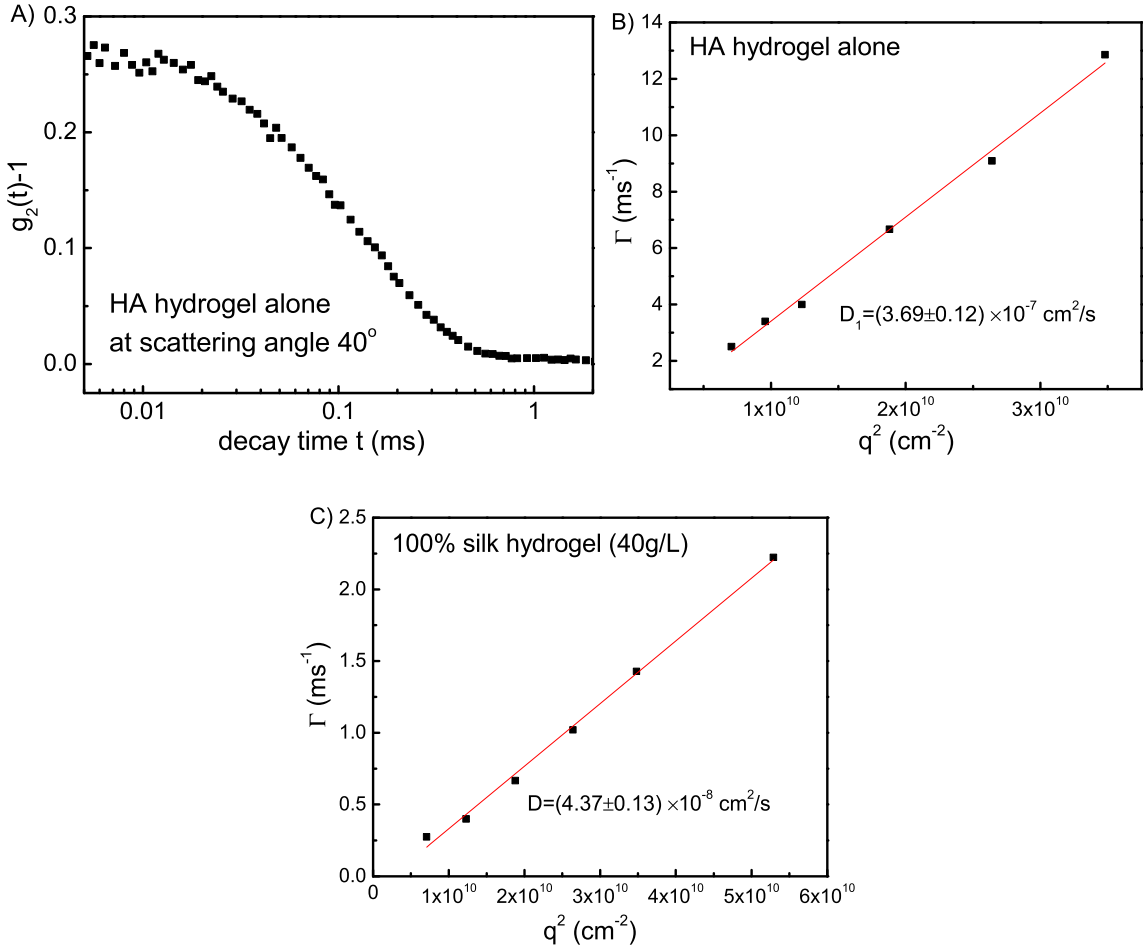

Fig. 6. (A) Intensity-intensity correlation function for HA hydrogel alone at scattering angle 40°. Fitting results of q^2 dependence of the relaxation rate Γ for HA hydrogel alone (B) and silk hydrogel alone (C).

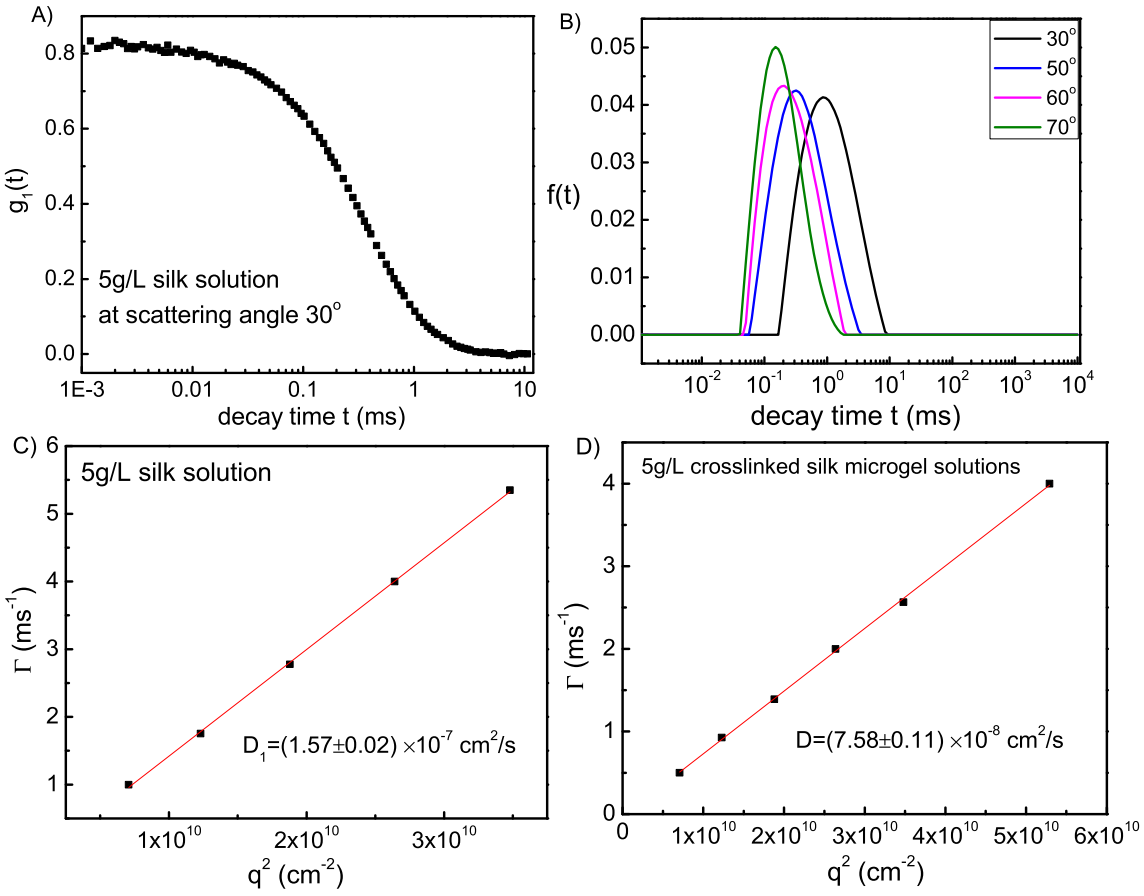

Fig. 7. (A) Intensity-intensity correlation function for 5 g/L silk solution at scattering angle 30°. (B) Corresponding relaxation time distribution function obtained from CONTIN fit at different scattering angles for the 5 g/L silk solution. (C), (D) Fitting results of q^2 dependence of the relaxation rate Γ for 5 g/L silk solution (C) and 5 g/L crosslinked silk microgel solutions (D).

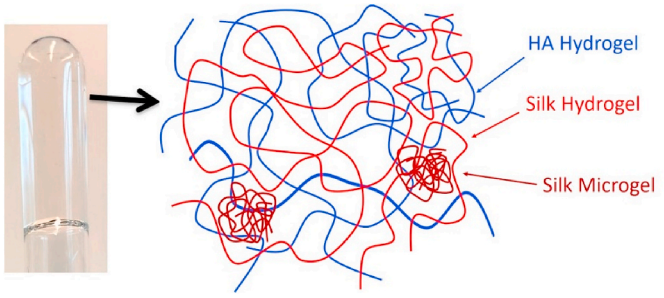

Fig. 8. Dynamic light scattering sample of 50S/50HA hydrogel composite (left) and the schematic illustration of the internal structure (right) of 50S/50HA hydrogel composite.

110 Pa, respectively. For the composite hydrogels, H_2O_2 concentration had a direct effect on the initial shear storage modulus. The modulus of hydrogels with no silk (0S/100H) did not change due to H_2O_2 concentration. Each ratio had different H_2O_2 concentrations independently chosen for the low, medium, and high mechanical ranges, as specified in Table 1. Hydrogels formed with the same concentration of H_2O_2 were used to determine changes due to polymeric ratio. Specifically, a H_2O_2 concentration of 0.05 × 10^{-2}% was utilized for 50S/50H low, 25S/75H medium, 10S/90H high, and 0S/100H high. For the composite hydrogels, decreasing silk concentration increased the initial storage modulus. It is possible that this result could be due to multiple factors. In this system (polymer concentration of 1% w/v diluted with HBSS), silk could not form a hydrogel alone. Therefore, decreasing the HA concentration and increasing silk concentration led to decreased mechanical strength in the composite hydrogels. However, when the silk was completely removed, the modulus decreased compared to the 10S/90H hydrogel. The inclusion of the shorter silk protein (~0.17 MDa [29]) in comparison to the larger HA polysaccharide (~0.9–1.0 MDa) may help to reduce steric hindrance and increase interchain crosslinking as seen with other multi-component systems [45,46].

It is important to understand any temporal changes in mechanical properties, as ideal vitreous substitutes need to be stable for extended periods of times, preferably over 3 months [7]. In previous experiments, we showed that enzymatically crosslinked silk hydrogels exhibited an increase in mechanics over time due to a conformational change from primarily random coil to beta sheet secondary structure, with changes starting as early as 2 weeks [16]. Increasing HA concentration in a silk-HA composite hydrogel prolonged and reduced this stiffening [16], presumably by increasing water content and shielding the hydrophobic domains in the silk chains to reduce their self-assembly into beta sheets. In this study, all samples exhibited stable mechanics after 1 month except that of the hydrogel with the largest silk ratio, 50S/50H, which had a 4×, 2×, and 1.6× increase in modulus for the low, medium, and high H_2O_2 concentrations. The larger changes in mechanics from lower H_2O_2 concentrations may be a result of lower crosslinking density and a less constrained hydrogel that better facilitates silk protein aggregation and beta sheet crystallization.

Both polymer ratio and H_2O_2 concentration affected the swelling properties of the hydrogels. Controlled swelling is important for vitreous humor substitutes, which is needed to maintain intraocular pressure and keep the retina in place [4,47]. The degree of swelling is related to crosslinking density, where a decrease in crosslinking density resulted in a less constrained network, allowing hydrogels to swell until

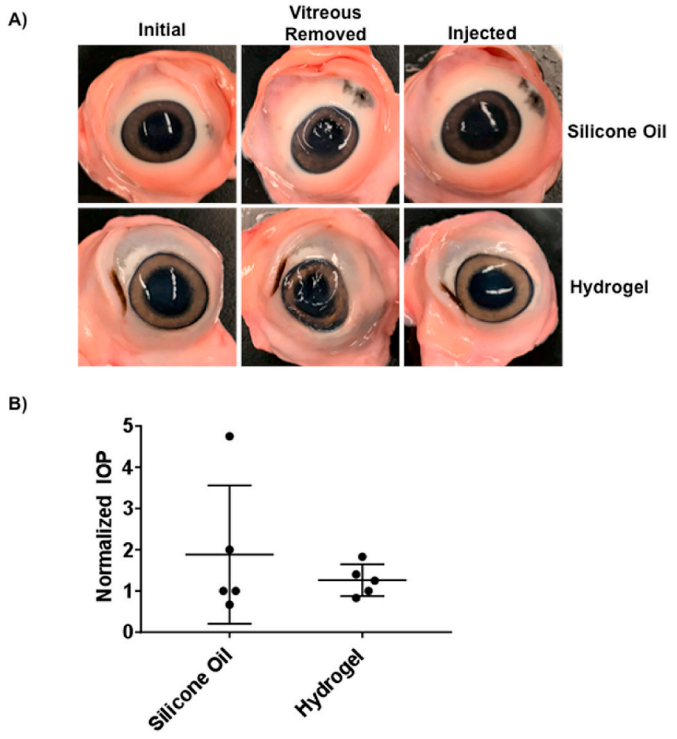

Fig. 9. *Ex Vivo* Injections. (A) Images of porcine eyes prior to vitreous removal (initial), after vitreous removal, and after injection with silicone oil or silk-HA hydrogel are shown. (B) Normalized IOP was not significantly different between the silicone oil and hydrogel injected eyes ($n = 5$, $p > 0.05$).

equilibrium is established. Therefore, the lower H_2O_2 concentrations for all composite hydrogels allowed for more swelling to occur. For the 50S/50H and 25S/75H ratios, high H_2O_2 concentration provided a highly constrained network, preventing any significant volumetric changes. Swelling is not only dependent on crosslinking density but also polymeric ratio. For the 50S/50H ratios, all hydrogels equilibrated after 15 days to their original volume, even if initial swelling was observed. The 50S/50H had a significantly lower volume when compared to polymer ratios with higher HA concentrations. This is similar to previous results that showed increased contents of the highly hydrophilic polymer, HA, increased water retention [16].

The 50S/50H hydrogel composite aging process was monitored by dynamic light scattering resulting in three modes: D_1 is hydrogel elastic diffusion from HA component, D_2 is hydrogel elastic diffusion from silk component and D_3 is from diffusion of silk microgel particles. D_1 and D_2 increased slightly with time, consistent with G' increasing with time. The volume of 50S/50H hydrogel composite decreased with time so that the gel network became tighter, diffusion of silk microgel particles in the hydrogel matrix became slower with time due to stronger confinement. These dynamic light scattering results are consistent with the mechanical and swelling properties of the hydrogel composite.

Another important parameter for vitreous humor substitutes is the optical properties. Optical transparency and refractive index similar to that of native vitreous humor is necessary to provide clear vision. The refractive indexes of the hydrogels are within previously reported ranged of native vitreous humor (1.334–1.337) [1,4]. The percentage of visible light transmitted initially and after 1 month, ranges between 75 and 91% depending on wavelength and time, which is a slight decrease from native vitreous at 85–95% light transmittance [15]. All hydrogels exhibited lower transmittance at lower wavelengths, which was similar to that of native vitreous, (~85% transmittance at 400 nm) and unlike silicone oil (100% transmittance at 400 nm) [15]. This reduced transmittance at lower wavelengths is advantageous as it helps to prevent damage to retinal epithelium [48]. At 1 month, only the 50S/50H low and 25S/75H low showed significant differences to visible wavelengths compared to the saline control. These samples had higher silk ratios along with less crosslinking density, which could have facilitated protein aggregation and crystallization causing the slight decrease in transparency [27,49].

The silk-HA composite hydrogel system characterized in this study shows promise as a vitreous humor substitute. Vitreous substitutes need to mimic native optical properties and provide tamponade to maintain retinal placement and intraocular pressure [3]. In this study we have shown that optically clear silk-HA hydrogels can be generated with a large range of mechanical and swelling properties through altering the polymeric ratio and crosslinking density with gelation time that is amenable for *in situ* gelation. In addition, preliminary *ex vivo* injections show restoration of ocular volume, similar to that of clinically used substitutes. Future directions involve determining longer term stability (> 3 months), retinal cell compatibility, *in vivo* responses, and modifying the hydrogels for use as a drug delivery vehicle. A potential limitation of this method is residual HRP in the hydrogels; a factor to be assessed before proceeding into animal studies.

Declaration of competing interest

None.

Acknowledgements

This work was supported by the NIH (P41EB027062, R01EB021264, R01NS092847) and the AFOSR FA9550-17-1-0333. The authors would like to thank Dr. Morgan Hawker, Dr. Annie Golding, Prof. Siwei Zhao, Prof. Mark Cronin-Golomb, Emily Eikhoff, and Dr. Laura Place for their assistance and imperative scientific advice.

Appendix A. Supplementary data

Supplementary data to this article can be found online at https://doi.org/10.1016/j.biomaterials.2019.119729.

Data availability statement

All data associated with this work will be provided upon request.

References

[1] T.V. Chirila, Y. Hong, Chapter C2 the vitreous humor, in: W. Murphy, J. Black, G. Hastings (Eds.), Handbook of Biomaterial Properties, Springer, New York, NY, 2016, pp. 125–134.
[2] E. Stefansson, Physiology of vitreous surgery, Graefe's archive for clinical and experimental ophthalmology = Albrecht von Graefes Archiv fur klinische und experimentelle Ophthalmologie 247 (2) (2009) 147–163.
[3] X. Su, M.J. Tan, Z. Li, M. Wong, L. Rajamani, G. Lingam, X.J. Loh, Recent progress in using biomaterials as vitreous substitutes, Biomacromolecules 16 (10) (2015) 3093–3102.
[4] K.E. Swindle-Reilly, M.A. Reilly, N. Ravi, 5 - current concepts in the design of hydrogels as vitreous substitutes, in: T.V. Chirila, D.G. Harkin (Eds.), Biomaterials and Regenerative Medicine in Ophthalmology, second ed., Woodhead Publishing, 2016, pp. 101–130.
[5] C.S. Nickerson, Engineering the Mechanical Properties of Ocular Tissues, California Institute of Technology, 2006.
[6] S. Santhanam, J. Liang, J. Struckhoff, P.D. Hamilton, N. Ravi, Biomimetic hydrogel with tunable mechanical properties for vitreous substitutes, Acta Biomater. 43 (2016) 327–337.
[7] T.T. Kleinberg, R.T. Tzekov, L. Stein, N. Ravi, S. Kaushal, Vitreous substitutes: a comprehensive review, Surv. Ophthalmol. 56 (4) (2011) 300–323.
[8] S. Donati, S.M. Caprani, G. Airaghi, R. Vinciguerra, L. Bartalena, F. Testa, C. Mariotti, G. Porta, F. Simonelli, C. Azzolini, Vitreous substitutes: the present and the future, BioMed Res. Int. 2014 (2014) 351804.
[9] J. Sebag, Vitreous: in Health and Disease, 1 ed., Springer, 2014.
[10] S. Maruoka, T. Matsuura, K. Kawasaki, M. Okamoto, H. Yoshiaki, M. Kodama, M. Sugiyama, M. Annaka, Biocompatibility of polyvinylalcohol gel as a vitreous substitute, Curr. Eye Res. 31 (7–8) (2006) 599–606.
[11] Y. Hong, T.V. Chirila, S. Vijayasekaran, W. Shen, X. Lou, P.D. Dalton, Biodegradation in vitro and retention in the rabbit eye of crosslinked poly(1-vinyl-

2-pyrrolidinone) hydrogel as a vitreous substitute, J. Biomed. Mater. Res. 39 (4) (1998) 650–659.
[12] F. Baino, Towards an ideal biomaterial for vitreous replacement: historical overview and future trends, Acta Biomater. 7 (3) (2011) 921–935.
[13] C. Schramm, M.S. Spitzer, S. Henke-Fahle, G. Steinmetz, K. Januschowski, P. Heiduschka, J. Geis-Gerstorfer, T. Biedermann, K.U. Bartz-Schmidt, P. Szurman, The cross-linked biopolymer hyaluronic acid as an artificial vitreous substitute, Investig. Ophthalmol. Vis. Sci. 53 (2) (2012) 613–621.
[14] D.F. Coutinho, S.V. Sant, H. Shin, J.T. Oliveira, M.E. Gomes, N.M. Neves, A. Khademhosseini, R.L. Reis, Modified Gellan Gum hydrogels with tunable physical and mechanical properties, Biomaterials 31 (29) (2010) 7494–7502.
[15] S. Suri, R. Banerjee, In vitro evaluation of in situ gels as short term vitreous substitutes, J. Biomed. Mater. Res. A 79 (3) (2006) 650–664.
[16] N.R. Raia, B.P. Partlow, M. McGill, E.P. Kimmerling, C.E. Ghezzi, D.L. Kaplan, Enzymatically crosslinked silk-hyaluronic acid hydrogels, Biomaterials 131 (2017) 58–67.
[17] S.A. Bradner, B.P. Partlow, P. Cebe, F.G. Omenetto, D.L. Kaplan, Fabrication of elastomeric silk fibers, Biopolymers 107 (9) (2017).
[18] J.E. Brown, B.P. Partlow, A.M. Berman, M.D. House, D.L. Kaplan, Injectable silk-based biomaterials for cervical tissue augmentation: an in vitro study, Am. J. Obstet. Gynecol. 214 (1) (2016) 118.e1–118.e9.
[19] G.-D. Kang, J.-H. Nahm, J.-S. Park, J.-Y. Moon, C.-S. Cho, J.-H. Yeo, Effects of poloxamer on the gelation of silk fibroin, Macromol. Rapid Commun. 21 (11) (2000) 788–791.
[20] U.J. Kim, J. Park, C. Li, H.J. Jin, R. Valluzzi, D.L. Kaplan, Structure and properties of silk hydrogels, Biomacromolecules 5 (3) (2004) 786–792.
[21] X. Leng, B. Liu, B. Su, M. Liang, L. Shi, S. Li, S. Qu, X. Fu, Y. Liu, M. Yao, D.L. Kaplan, Y. Wang, X. Wang, In situ ultrasound imaging of silk hydrogel degradation and neovascularization, J. Tissue Eng. Regenerat. Med. 11 (3) (2017) 822–830.
[22] M. McGill, J.M. Coburn, B.P. Partlow, X. Mu, D.L. Kaplan, Molecular and macroscale analysis of enzyme-crosslinked silk hydrogels for rational biomaterial design, Acta Biomater. 63 (2017) 76–84.
[23] B.P. Partlow, C.W. Hanna, J. Rnjak-Kovacina, J.E. Moreau, M.B. Applegate, K.A. Burke, B. Marelli, A.N. Mitropoulos, F.G. Omenetto, D.L. Kaplan, Highly tunable elastomeric silk biomaterials, Adv. Funct. Mater. 24 (29) (2014) 4615–4624.
[24] W.L. Stoppel, A.E. Gao, A.M. Greaney, B.P. Partlow, R.C. Bretherton, D.L. Kaplan, L.D. Black 3rd, Elastic, silk-cardiac extracellular matrix hydrogels exhibit time-dependent stiffening that modulates cardiac fibroblast response, J. Biomed. Mater. Res. A 104 (12) (2016) 3058–3072.
[25] X. Wang, J.A. Kluge, G.G. Leisk, D.L. Kaplan, Sonication-induced gelation of silk fibroin for cell encapsulation, Biomaterials 29 (8) (2008) 1054–1064.
[26] T. Yucel, P. Cebe, D.L. Kaplan, Vortex-induced injectable silk fibroin hydrogels, Biophys. J. 97 (7) (2009) 2044–2050.
[27] S. Zhao, Y. Chen, B.P. Partlow, A.S. Golding, P. Tseng, J. Coburn, M.B. Applegate, J.E. Moreau, F.G. Omenetto, D.L. Kaplan, Bio-functionalized silk hydrogel microfluidic systems, Biomaterials 93 (2016) 60–70.
[28] M.L. Lovett, X. Wang, T. Yucel, L. York, M. Keirstead, L. Haggerty, D.L. Kaplan, Silk hydrogels for sustained ocular delivery of anti-vascular endothelial growth factor (anti-VEGF) therapeutics, Eur. J. Pharm. Biopharm. : Off. J. Arbeitsgemeinschaft fur Pharmazeutische Verfahrenstechnik e.V 95 (Pt B) (2015) 271–278.
[29] B.P. Partlow, A.P. Tabatabai, G.G. Leisk, P. Cebe, D.L. Blair, D.L. Kaplan, Silk fibroin degradation related to rheological and mechanical properties, Macromol. Biosci. 16 (5) (2016) 666–675.
[30] J.E. Brown, C.P. Gulka, J.E.M. Giordano, M.P. Montero, A. Hoang, T.L. Carroll, Injectable silk protein microparticle-based fillers: a novel material for potential use in glottic insufficiency, J. Voice : Off. J. Voice Found. 33 (5) (2019) 773–780.
[31] M. Kurisawa, F. Lee, L.-S. Wang, J.E. Chung, Injectable enzymatically crosslinked hydrogel system with independent tuning of mechanical strength and gelation rate for drug delivery and tissue engineering, J. Mater. Chem. 20 (26) (2010) 5371–5375.
[32] F. Lee, J.E. Chung, M. Kurisawa, An injectable enzymatically crosslinked hyaluronic acid,Äityramine hydrogel system with independent tuning of mechanical strength and gelation rate, Soft Matter 4 (4) (2008) 880–887.
[33] D.N. Rockwood, R.C. Preda, T. Yucel, X. Wang, M.L. Lovett, D.L. Kaplan, Materials fabrication from Bombyx mori silk fibroin, Nat. Protoc. 6 (10) (2011) 1612–1631.
[34] D. Jia, M. Muthukumar, H. Cheng, C.C. Han, B. Hammouda, Concentration fluctuations near lower critical solution temperature in ternary aqueous solutions, Macromolecules 50 (18) (2017) 7291–7298.
[35] D. Jia, M. Muthukumar, Topologically frustrated dynamics of crowded charged macromolecules in charged hydrogels, Nat. Commun. 9 (1) (2018) 2248.
[36] C.C. Han, A.Z. Akcasu, Scattering and Dynamics of Polymers: Seeking Order in Disordered Systems, John Wiley & Sons, Singapore, 2011.
[37] S.W. Provencher, CONTIN: a general purpose constrained regularization program for inverting noisy linear algebraic and integral equations, Comput. Phys. Commun. 27 (3) (1982) 229–242.
[38] D. Jia, M. Muthukumar, Effect of salt on the ordinary-extraordinary transition in solutions of charged macromolecules, J. Am. Chem. Soc. 141 (14) (2019) 5886–5896.
[39] S. Morozova, M. Muthukumar, Elasticity at swelling equilibrium of ultrasoft polyelectrolyte gels: comparisons of theory and experiments, Macromolecules 50 (6) (2017) 2456–2466.
[40] C.Z. Zhou, F. Confalonieri, M. Jacquet, R. Perasso, Z.G. Li, J. Janin, Silk fibroin: structural implications of a remarkable amino acid sequence, Proteins 44 (2) (2001) 119–122.
[41] C. Alovisi, C. Panico, U. de Sanctis, C.M. Eandi, Vitreous substitutes: old and New materials in vitreoretinal surgery, J. Ophthalmol. 2017 (2017) 3172138.
[42] F. Baino, The use of polymers in the treatment of retinal detachment: current trends and future perspectives, Polymers 2 (3) (2010) 286.
[43] J.A. Zimberlin, J.J. McManus, A.J. Crosby, Cavitation rheology of the vitreous: mechanical properties of biological tissue, Soft Matter 6 (15) (2010) 3632–3635.
[44] M. Annaka, K. Mortensen, M.E. Vigild, T. Matsuura, S. Tsuji, T. Ueda, H. Tsujinaka, Design of an injectable in situ gelation biomaterials for vitreous substitute, Biomacromolecules 12 (11) (2011) 4011–4021.
[45] A. Khanlari, J.E. Schulteis, T.C. Suekama, M.S. Detamore, S.H. Gehrke, Designing crosslinked hyaluronic acid hydrogels with tunable mechanical properties for biomedical applications, J. Appl. Polym. Sci. 132 (22) (2015).
[46] K.Y. Lee, J.A. Rowley, P. Eiselt, E.M. Moy, K.H. Bouhadir, D.J. Mooney, Controlling mechanical and swelling properties of alginate hydrogels independently by cross-linker type and cross-linking density, Macromolecules 33 (11) (2000) 4291–4294.
[47] W.J. Foster, Vitr. Substit. Expert Rev. Ophthalmol. 3 (2) (2008) 211–218.
[48] J.R. Sparrow, K. Nakanishi, C.A. Parish, The lipofuscin fluorophore A2E mediates blue light-induced damage to retinal pigmented epithelial cells, Investig. Ophthalmol. Vis. Sci. 41 (7) (2000) 1981–1989.
[49] V.P. Ribeiro, J. Silva-Correia, C. Goncalves, S. Pina, H. Radhouani, T. Montonen, J. Hyttinen, A. Roy, A.L. Oliveira, R.L. Reis, J.M. Oliveira, Rapidly responsive silk fibroin hydrogels as an artificial matrix for the programmed tumor cells death, PLoS One 13 (4) (2018) e0194441.